Analysis, Design, and Implementation of a High Gain Soft-Switching Bidirectional DC–DC Converter With PPS Control

Hyeonju Jeong, Minho Kwon, and Sewan Choi, *Senior Member, IEEE*

***Abstract*—This paper proposes a pulse width modulation plus phase-shift (PPS) control for nonisolated high gain soft-switching bidirectional dc–dc converter (HSBDC). The phase-shift angle is used to control the direction and amount of power flow of the bidirectional dc–dc converter, while the duty cycle is used to balance the voltage between two high voltage side (HVS) capacitors. The HSBDC with PPS control has the advantages of simple control structure and symmetrical switching patterns, ensured soft-switching in both forward and backward modes at all load under wide voltage range, and reduced voltage ratings of the HVS capacitors and switches. The operation principle of the HSBDC with PPS control is analyzed in detail. Based on the analysis the passive component is designed to achieve higher efficiency. A 3-kW prototype is implemented and tested to verify the validity of the proposed method.**

***Index Terms*—Bidirectional dc–dc converter, high step-up/down, high gain, pulse width modulation (PWM) plus phase-shift (PPS), soft-switching.**

I. Introduction

As THE issues of environmental problems have gained greater visibility, several research works have been performed for efficient and ecofriendly utilization of energy in a wide range of applications, such as energy storage systems, hybrid electric vehicles, and uninterruptible power supplies. The bidirectional dc–dc converter is placed between the dc link and energy storage devices such as batteries or supercapacitors and plays a significant role in controlling the power flow and/or voltage in these systems.

The cell voltage of a battery or supercapacitor is inherently low; therefore, individual cells are stacked up in series to meet the required voltage level. A battery management system (BMS) must be used to correct the cell imbalance caused by different properties of the cell, which may result in rapid aging and inefficient utilization of the energy storage cell. Therefore, in order to reduce the cost burden of BMS, a low voltage is preferred for energy storage devices [1]–[4]. A nonisolated dc–dc converter is preferred for higher efficiency and power density if galvanic isolation is not essential [5], [6]. The conventional half-bridge (HB) converter has been commonly used as a nonisolated bidirectional dc–dc converter. The main advantages of the conventional HB converter are simple structure and low cost due to low component count and simple drive circuitry [6]. However, the effective step-up voltage gain is reduced due to voltage drops on the switches and parasitic components of the inductor and capacitor. Further use of extreme duty cycles for high step-up/down operations leads to short-pulsed currents with high amplitudes flowing through the diode, which causes serious reverse recovery problems [7]. Therefore, when voltage of energy storage devices is low the nonisolated bidirectional dc–dc converter with high step-up/down gain is required.

Several nonisolated bidirectional converters with high step-up/down gain have been introduced in the literatures [8]–[18]. A three-level dc–dc converter with extended step-up/down gain was proposed in [8], which has the merits of a simple structure. The switched-capacitor type dc–dc converter [8]–[12] enlarges the step-up/down gain without using an extreme duty cycle; however, it requires high switch and capacitor counts. The coupled-inductor type dc–dc converter [13]–[18] is able to obtain high step-up/down gain without using an extreme duty cycle by utilizing turns ratio of the coupled inductor. However, the current ripple on the low voltage side (LVS) is large due to the operation of the coupled inductor. In addition, the problem associated with the leakage inductor induces a considerable voltage stress on the switching devices. Furthermore, there is a restriction on operating the converter at high switching frequency for reducing its volume and weight because hard switching introduces switching losses and electromagnetic interference noises.

Recently, two attractive bidirectional topologies suitable for high step-up/down application were presented in [19] and [21]. Series capacitor based topology proposed in [19] provides relatively high conversion ratio (from 8 to 13.5) and achieves zero voltage switching (ZVS) turn-on. A frequency modulation strategy was employed for reducing current stress and conduction losses. However, due to limited duty cycle, a precharging technique for the series capacitors is required to overcome the start-up issue [20]. Coupled-inductor-based topology in [21] employs pulse width modulation (PWM) plus phase-shift (PPS) control method. A phase-shift angle is used to regulate power flow of the topology, while a duty cycle is used to reduce circulating current and to achieve soft-switching of all switches. However, this topology also suffers from the drawbacks inherent in coupled

Manuscript received December 19, 2016; revised March 28, 2017 and June 14, 2017; accepted July 26, 2017. Date of publication August 11, 2017; date of current version February 22, 2018. This work was supported by the National Research Foundation of Korea (NRF) grant funded by the Korea government (MSIP) (2017R1A2A2A05001054). Recommended for publication by Associate Editor G. Moschopoulos. *(Corresponding author: Sewan Choi.)*

H. Jeong, M. Kwon and S. Choi are with the Department of Electrical & Information Engineering, Seoul National University of Science and Technology, Seoul 139-743 Korea. (e-mail: hyeonju0618@seoultech.ac.kr; byeonggill@seoultech.ac.kr; schoi@seoultech.ac.kr).

Color versions of one or more of the figures in this paper are available online at http://ieeexplore.ieee.org.

Digital Object Identifier 10.1109/TPEL.2017.2738705

inductors such as large current ripple on LVS and difficulty of identical manufacturing.

A high gain soft-switching bidirectional dc–dc converter (HSBDC) with a PWM control [22] was introduced for high step-up/down applications. The PWM control method aims at optimizing switching characteristics by controlling delay times for switches, but gives rise to asymmetrical operation in the forward and backward modes. The issues on the PWM control method associated with asymmetrical switching patterns are as follows.

1) In order to achieve soft-switching the delay times must *vary continuously according to load and voltage variation*, which increases burden to the micro controller unit (MCU) and complexity of switching pattern generation. The required delay times for soft-switching should be increased as the load power or voltage gain increase, which results in increased voltage unbalance between capacitors on the high voltage side (HVS). This, in turn, increases voltage stress of the HVS capacitors and switches.
2) In the backward mode, the delay time for S_2 *narrows* the range of step-down gain. Therefore, especially, in the *wide* voltage range application the reduced effective step-down gain significantly limits the usable delay time, resulting in *soft-switching failure*.
3) The auxiliary inductor is the most crucial component that affects performance of the HSBDC. In the forward mode the larger the auxiliary inductance is, the wider the soft-switching range is. However, due to *asymmetrical switching* between forward and backward modes the increased auxiliary inductance for wider soft-switching range in the forward mode narrows the soft-switching range in the backward mode. This may cause *a sacrifice of soft-switching* either in the forward *or* backward mode.

This paper proposes a PPS control for nonisolated soft-switching bidirectional dc–dc converter to overcome the above-mentioned problems. The proposed PPS method uses two control variables, phase-shift angle ϕ and duty cycle D. The phase shift angle is used to control the direction and amount of power flow while the duty cycle is used to balance the voltage between two capacitors on the HVS, which gives the following advantages over the PWM control method used in [22].

1) The voltage ratings of the HVS capacitors and switches become *exactly half* of the HVS voltage. Balancing the capacitor voltages makes shape of the auxiliary inductor current "flat" at all load and voltage conditions, resulting in *guaranteed ZVS turn-on over the whole ranges* of the load power and voltage step-up gain.
2) In the meantime, delay times are not required for the proposed PPS method. Therefore, the effective step-up/down gain is not affected by load and voltage variation, thereby ensuring *soft-switching at all load and voltage conditions*.
3) The larger the auxiliary inductance is, the wider the soft-switching range is. Due to "symmetrical" switching between forward and backward modes the increased auxiliary inductance for wider soft-switching range in the forward mode does not narrow the soft-switching range in the backward mode, thereby *not* requiring *a sacrifice of soft-switching either in the forward or backward mode.*

In summary, compared with the PWM control method, the proposed PPS method has following the advantages: 1) simple control structure and symmetrical switching patterns, 2) ensured soft-switching in both forward and backward modes at all load and voltage conditions, and 3) identical voltage ratings of the HVS capacitors and switches.

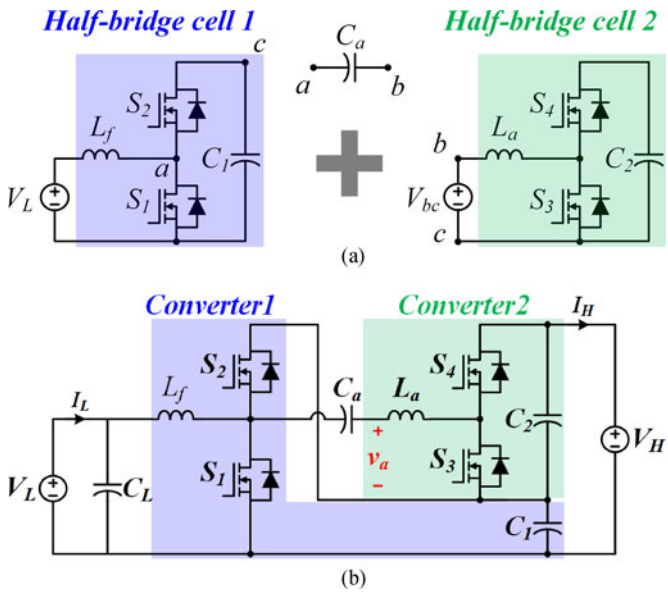

Fig. 1. Circuit diagram. (a) Concept of the topology derivation. (b) HSBDC.

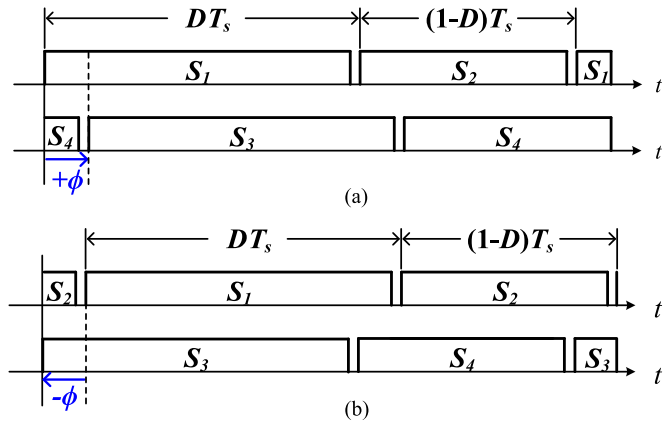

Fig. 2. PPS switching method for the HSBDC. (a) Forward operation. (b) Backward operation.

The operation principle of the HSBDC with PPS control is analyzed in detail. Based on the analysis the passive component is designed to achieve higher efficiency.

II. Operating Principles

Fig. 1 shows the circuit diagram of the HSBDC. Fig. 1(a) shows the concept of topology derivation of the HSBDC where two HB cells are connected via auxiliary capacitor C_a in such a way that two output capacitors C_1 and C_2 are connected in series to obtain high step-up gain, resulting in the HSBDC, as shown in Fig. 1(b).

Fig. 2 shows the PPS switching method for the HSBDC. The LVS switches S_1 and S_2 are operated under asymmetrical complementary switching with duty cycles of D and $1-D$, respectively. Similarly, the HVS switches S_3 and S_4 are operated under asymmetrical complementary switching with duty cycles

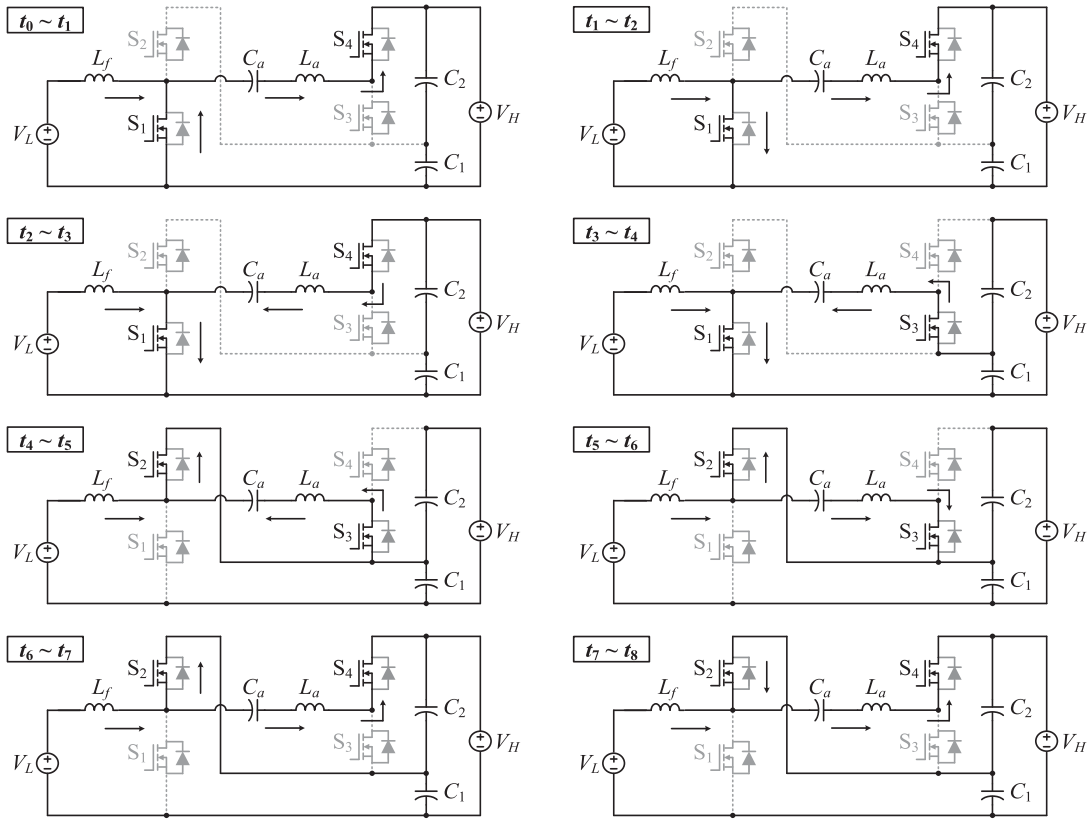

Fig. 3. Operation stages of the HSBDC with PPS control for forward operation.

of D and $1-D$, respectively. The phase-shift angle ϕ is defined as the phase difference between the gate drive signals of S_1 and S_3, and is used to control the direction and amount of the delivered power. In the forward mode, as shown in Fig. 2(a), the gate drive signal for S_1 leads that for S_3 ($\phi > 0$), so that power is delivered from the LVS to the HVS. On the contrary, in the backward mode, as shown in Fig. 2(b), the gate drive signal for S_1 lags that for S_3 ($\phi < 0$), so that power is delivered from the HVS to the LVS. In this paper, the phase-shift angle ϕ is represented as a percentage of switching period T_s.

The operating principles of the forward and backward modes of the HSBDC with PPS control are described in detail. The operation modes and key waveforms of the HSBDC with PPS control for forward operation are shown in Figs. 3 and 4, respectively. The switching cycle can be divided into eight stages, which are explained as follows.

1) Mode 1 $[t_0 - t_1]$: This mode begins when S_2, which was carrying the difference in current between i_{La} and i_{Lf}, is turned OFF. The gating signal for S_1 is applied during this mode, and S_1 is turned ON under the ZVS condition. Inductor currents i_{La} and i_{Lf} start to decrease and increase, respectively, with the slopes determined by the following equations:

$$\frac{di_{La}}{dt} = \frac{V_{Ca} - V_{C1} - V_{C2}}{L_a} \tag{1}$$

$$\frac{di_{Lf}}{dt} = \frac{V_L}{L_f}. \tag{2}$$

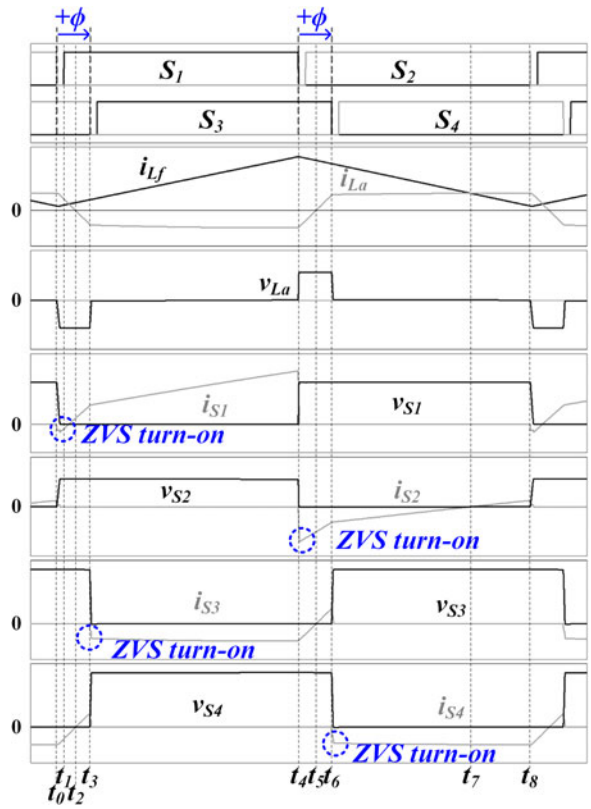

Fig. 4. Key waveforms of the HSBDC with PPS control for forward operation.

2) Mode 2 $[t_1 - t_2]$: When the increasing current i_{Lf} becomes greater than the decreasing current i_{La}, the current flowing through S_1 is reversed. During this mode, i_{La} and i_{Lf} keep flowing with the same slope determined in Mode 1.
3) Mode 3 $[t_2 - t_3]$: This mode begins when i_{La} is reversed. Both the inductor currents i_{Lf} and i_{La} flows through S_1. During this mode, i_{La} and i_{Lf} keep flowing with the same slope determined in Mode 1.
4) Mode 4 $[t_3 - t_4]$: This mode begins when S_4, which was carrying i_{La} is turned OFF. The gating signal for S_3 is applied during this mode, and S_3 is turned ON under ZVS condition. V_{Ca} is equal to V_{C1}, therefore, the slope of the current flowing through L_a is zero, which means that i_{La} is constant in this mode.
5) Mode 5 $[t_4 - t_5]$: This mode begins when S_1, which was carrying both i_{La} and i_{Lf}, is turned OFF. The gating signal for S_2 is applied during this mode, and S_2 is turned ON under ZVS condition. Both i_{La} and i_{Lf} start to decrease, with the slopes determined by the following equations:

$$\frac{di_{La}}{dt} = \frac{V_{Ca}}{L_a} \tag{3}$$

$$\frac{di_{Lf}}{dt} = \frac{V_L - V_{C1}}{L_f}. \tag{4}$$

6) Mode 6 $[t_5 - t_6]$: This mode begins when i_{La} is reversed. The difference in current between i_{Lf} and i_{La} flows through S_2. During this mode, i_{La} and i_{Lf} keep flowing with the same slope determined in Mode 5.
7) Mode 7 $[t_6 - t_7]$: This mode begins when S_3, which was carrying i_{La}, is turned OFF. The gating signal for S_4 is applied during this mode, and S_4 is turned ON under ZVS condition. V_{Ca} is equal to V_{C2}, therefore, the slope of the current flowing through L_a is zero, which means that i_{La} is constant in this mode.
8) Mode 8 $[t_7 - t_8]$: When the decreasing current i_{Lf} becomes smaller than constant current i_{La}, the current flowing through S_2 is reversed. During this mode, i_{Lf} keeps flowing with the same slope determined in Mode 5, while i_{La} remains constant. This is the end of the switching cycle. At t_0, S_2 is turned OFF, and this switching cycle is repeated.

Detailed explanation of operation modes and key waveforms of the HSBDC with PPS control for backward operation is omitted here, since the operating principle of the backward operation is symmetrical to the forward operation.

III. Analysis and Design

A. Voltage Step-Up/Down Gain

To obtain both the optimal duty and step-up/down gain of the HSBDC with PPS control, it is assumed that voltages across C_1, C_2, and C_a are constant during the switching period T_s. The output voltage is given by

$$V_H = V_{C1} + V_{C2}. \tag{5}$$

As shown in Fig. 1, V_{C1} and V_{C2} are the output voltages of HB 1 and HB 2, respectively. Therefore, they can be expressed as follows:

$$V_{C1} = \frac{1}{1-D} V_L \tag{6}$$

$$V_{C2} = \frac{1}{1-D} V_{bc}. \tag{7}$$

The average value of the voltage across the inductor is zero, therefore

$$V_L + V_{Ca} = V_{bc} + V_{C1}. \tag{8}$$

From (7) and (8), V_{C2} can be expressed as follows:

$$V_{C2} = \frac{1}{1-D}\left(V_L + V_{Ca} - V_{C1}\right). \tag{9}$$

Substituting (6) and (9) into (5), V_H can be expressed as follows:

$$V_H = \frac{2}{1-D} V_L + \frac{1}{1-D}\left(V_{Ca} - V_{C1}\right). \tag{10}$$

It is noted from Fig. 4 that letting $V_{Ca} - V_{C1}$ and $V_{C2} - V_{Ca}$ be zero increases the ZVS range for the switches S_3 and S_4, which leads to

$$V_{C1} = V_{C2} = V_{Ca}. \tag{11}$$

In addition, this makes the voltage ratings of the switches and capacitors equal, unlike the PWM switching method in [22]. From (10) and (11), the step-up/down gain of the converter becomes

$$V_H = \frac{2}{1-D} V_L. \tag{12}$$

Finally, the desired duty cycle of switches S_1 and S_3 can be obtained as follows:

$$D = 1 - \frac{2V_L}{V_H}. \tag{13}$$

B. Power Equations

The power equation can be expressed as follows:

$$P = V_H I_H. \tag{14}$$

From the waveforms of the forward mode in Fig. 4, the average value of i_{S4} can be calculated as follows:

$$I_{S4} = \frac{\phi\left(\phi + 2D^2 - 2D\right) V_H}{4L_a f_s}. \tag{15}$$

Since I_{S4} and I_H are the same in magnitude, the power equation of forward mode can be obtained as follows:

$$P = \phi\left(2D - 2D^2 - \phi\right)\frac{{V_H}^2}{4L_a f_s} \quad (\phi > 0). \tag{16}$$

The power equation of the backward mode can be calculated in the same way and expressed as follows:

$$P = \phi\left(2D - 2D^2 + \phi\right)\frac{{V_H}^2}{4L_a f_s} \quad (\phi < 0). \tag{17}$$

The power equation is a quadratic function of the phase-shift angle ϕ. Using (16) and (17), the power curve of the converter with respect to the phase-shift angle ϕ is plotted as shown

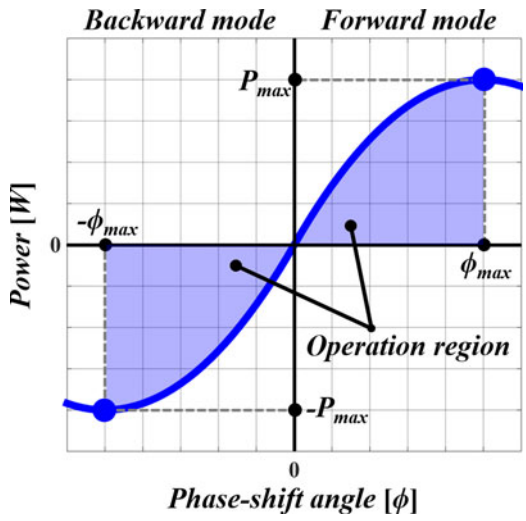

Fig. 5. Power curves versus phase-shift angle.

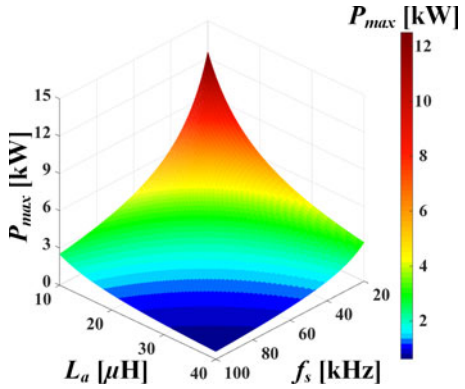

Fig. 6. Maximum transferred power versus L_a and f_s.

in Fig. 5. Note that the power is inversely proportional to L_a and f_s.

In the forward (backward) mode, the maximum transferred power $P_{\max}$ $(-P_{\max})$ occurs at the maximum available phase-shift angle $\phi_{\max}$ $(-\phi_{\max})$. Therefore, the regulating range of the phase-shift angle ϕ of the converter is from $-\phi_{\max}$ to $\phi_{\max}$. From (16), $\phi_{\max}$ and $P_{\max}$ can be obtained as follows:

$$\phi_{\max} = D - D^2 \tag{18}$$

$$P_{\max} = \left(D - D^2\right) \frac{{V_H}^2}{4L_a f_s}. \tag{19}$$

In addition, due to the symmetrical operation of the converter in both forward and backward modes, $-\phi_{\max}$ and $-P_{\max}$ in the backward mode are equal in magnitude but opposite in sign to those in the forward mode. Using (19), the maximum transferred power $P_{\max}$ as a function of L_a and f_s is plotted as shown in Fig. 6.

C. Design of Passive Components

In this section, the design procedure for the HSBDC with PPS control is presented with an example. A specification for the design example is given as follows: output power $P =$ 3000 W, LVS voltage $V_L =$ 86–116 V, HVS voltage $V_H =$ 390–450 V, current ripple of filter inductor $\Delta I_{Lf} =$ 30 A, and switching frequency $f_s =$ 50 kHz.

Step 1) Filter inductor L_f: The filter inductance can be obtained as follows:

$$L_f = \frac{DV_L}{\Delta I_{LF} f_s} = 37.5\ \mu\text{H} \tag{20}$$

where $V_L =$ 112.5 V, since the maximum ripple occurs at $D =$ 0.5 and $V_H =$ 450 V.

Step 2) Auxiliary inductor L_a: The auxiliary inductor L_a is a critical design parameter that affects soft-switching, rms current, and maximum transferred power.

In the forward mode, S_1 may not achieve ZVS turn-on since the turn-on current for ZVS is determined by the difference between auxiliary and filter inductor currents, while S_2 always achieve ZVS turn-on since the turn-on current for ZVS that is determined by the summation of auxiliary and filter inductor currents flowing through the body diode of S_2. In the backward mode, S_2 may not achieve ZVS turn-on, while S_1 always achieves ZVS turn-on. Due to the symmetrical operation of forward and backward modes, the ZVS turn-on condition for S_1 in the forward mode is the same as that for S_2 in the backward mode. Therefore, only the ZVS condition of S_1 in the forward mode is considered for the design of auxiliary inductance. In the forward mode, the turn-on current for S_1 at full load can be obtained by

$$i_{S1}(t_0) = i_{La}(t_0) - i_{Lf}(t_0) = \frac{V_H}{2L_a} \cdot \phi D T_s - \left(\frac{P}{V_L} - \frac{1}{2}\frac{V_L D}{L_f f_s}\right). \tag{21}$$

From Fig. 4, the rms current of the auxiliary inductor L_a can be obtained by

$$I_{La,rms} = \frac{1}{6}\frac{\phi V_H T_s \sqrt{9D - 9D^2 - 3\phi}}{L_a}. \tag{22}$$

Using (21) and (22), the turn-on current for S_1 and the rms current of the auxiliary inductor L_a as a function of auxiliary inductor L_a, can be plotted as shown in Figs. 7 and 8, respectively.

It can be seen in Fig. 7 that increasing L_a makes the ZVS turn-on easier. Meanwhile, Fig. 8 shows that increasing L_a increases the rms current of the auxiliary inductor, which not only leads to increased conduction losses, but reduced maximum transferred power $P_{\max}$. Therefore, considering the parasitic output capacitance of the MOSFET, the auxiliary inductance is selected to be 12 μH.

Step 3) Auxiliary capacitor C_a: In order to avoid resonance between L_a and C_a, the auxiliary capacitance C_a should be selected such that it is sufficiently large. In this design example, the auxiliary capacitance is selected to be 30 μF, so that the resonant frequency is smaller than one-fifth of the switching frequency.

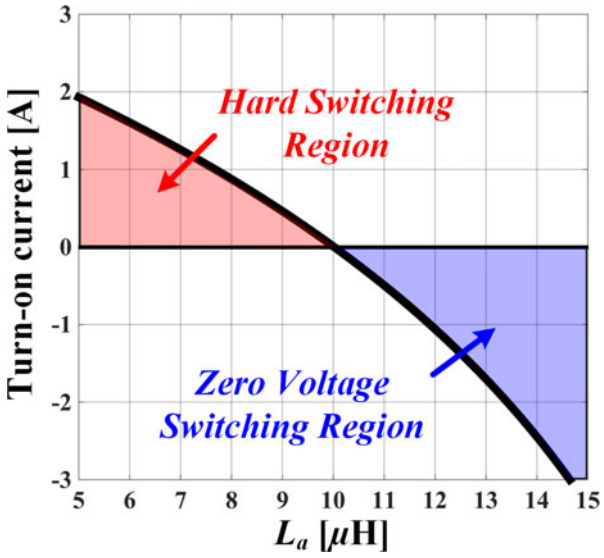

Fig. 7. Turn-on current versus auxiliary inductance under $P = 3$ kW, $V_L = 86$ V, and $V_H = 450$ V.

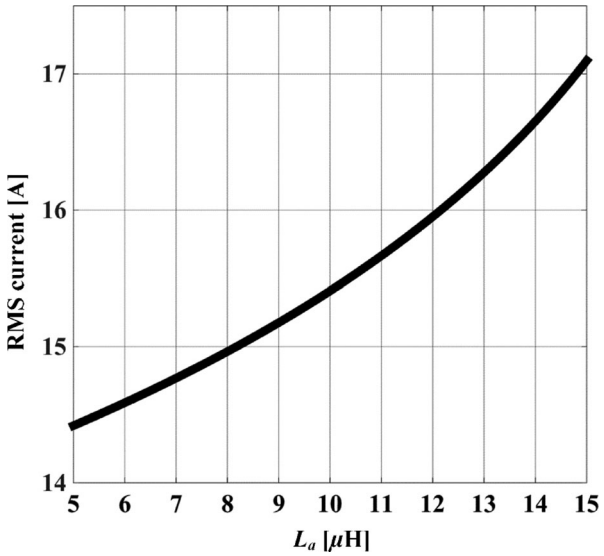

Fig. 8. RMS current versus auxiliary inductance under $P = 3$ kW, $V_L = 86$ V, and $V_H = 450$ V.

D. Design Comparison

In this section, the HSBDC with PPS control and conventional HB converter are designed under a specification and design results are compared. The design specification is given as follow: output power $P = 3000$ W, LVS voltage $V_L = 86$–116 V, HVS voltage $V_H = 390$–450 V, current ripple of filter inductor $\Delta I_{Lf} = 30$ A, $\Delta V_H = 10$ V, and switching frequency $f_s = 50$ kHz. The passive components values are obtained by $L_f = 37.5\,\mu$H, $L_a = 12\,\mu$H, and $C_{a,1,2} = 30\,\mu$F. Table I shows a comparison results on design of the HSBDC with PPS control and the conventional HB converter. It should be noted that a duty cycle of 0.41–0.62 was used for the HSBDC with PPS control to achieve a voltage gain of 3.6–5.2, while a duty cycle of 0.7–0.8 is used for the conventional HB converter to achieve the same voltage gain. Although numbers of switches and capacitors of the HSBDC with PPS control are higher than those of the conventional HB converter, voltage ratings of the components are half compared to the conventional HB converter, thereby making selection of the components more flexible. Besides, total energy volume of the inductors of the HSBDC with PPS control is smaller than that of the conventional converter due to smaller volt-second across the filter inductor of the HSBDC with PPS control.

TABLE I
COMPARISON OF THE HSBDC WITH PPS CONTROL AND THE CONVENTIONAL HB CONVERTER

	HSBDC with PPS control	Conventional HB converter
Switching frequency	50 kHz	50 kHz
Switching characteristic	ZVS turn-on	Hard switching
Voltage gain	$\frac{2}{1-D}$	$\frac{1}{1-D}$
Duty cycle range	0.41–0.62	0.7–0.8
Switches	S_1: 225 V/ 40 Arms S_2: 225 V/18 Arms S_3: 225 V/13 Arms S_4: 225 V/14 Arms	S_1: 450 V/32.7 Arms S_2: 450 V/15.8 Arms
Capacitor	$C_{1,2}$: 30 μF/ 225 V/ 10 A C_a : 30 μF/ 225 V/ 20 A	C_H : 12 μF/ 450 V/ 12.1 A
Inductor	L_f : 37.5 μH/ 36 A L_a : 12 μH/ 20 A	L_f : 57.4 μH/ 36 A
Total energy volume	26.7 mJ	37.2 mJ

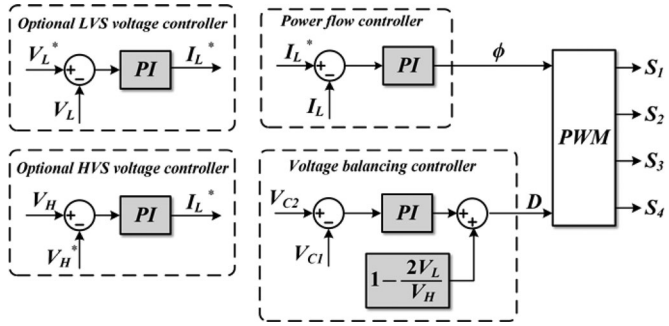

Fig. 9. Control block diagram of the HSBDC with PPS control.

IV. CONTROL STRATEGY

Fig. 9 shows the control block diagram of the HSBDC with PPS control. The power flow is regulated by controlling the phase-shift angle ϕ, which may be either positive or negative. When the phase-shift angle ϕ is positive, the power is delivered from the LVS to the HVS and when ϕ is negative, the power is delivered from the HVS to the LVS. Owing to the symmetrical operation of both the forward and backward modes, seamless power flow change can be achieved by using only the phase-shift angle ϕ. The optional voltage controller can be implemented as the outer loop of the power flow controller to regulate LVS or HVS voltage. The duty cycle D is controlled to balance the voltages V_{C1} and V_{C2}. Balancing of the voltages helps to not only equalize the voltage rating of all switches, but also to increase the ZVS range for the switches S_3 and S_4. In addition, (13) can be used as a feed-forward term in duty control.

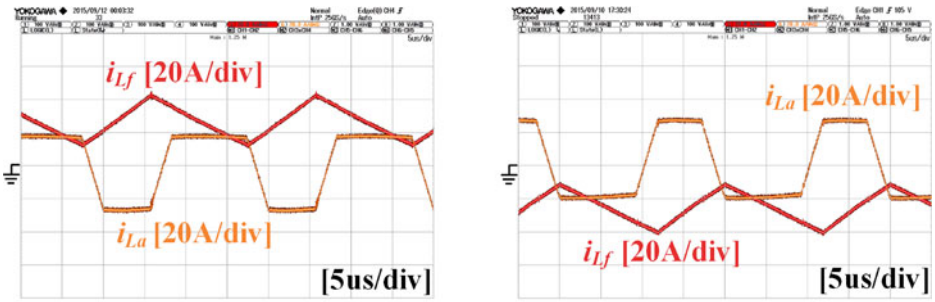

Fig. 10. Experimental waveforms of filter and auxiliary inductor currents at full load with $V_L = 116$ V and $V_H = 390$ V. (a) Forward mode. (b) Backward mode.

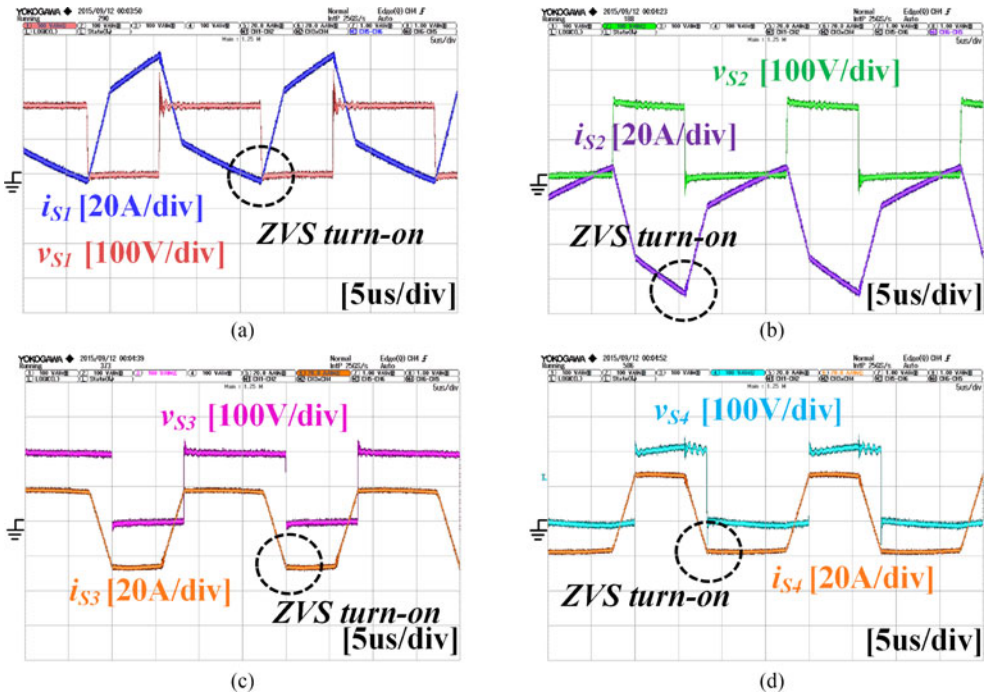

Fig. 11. Experimental waveforms of switch voltage and current in forward mode at full load with $V_L = 116$ V and $V_H = 390$ V. (a) S_1. (b) S_2. (c) S_3. (d) S_4.

V. Experimental Results

A 3-kW laboratory prototype was built and tested to verify the validity of the HSBDC with PPS control. The design specification and passive components values for experiment are the same as that used in Section IV-D. Also, experimental comparison between the PPS and PWM switching methods is provided.

The switches were implemented using 300 V-class MOSFETs (IXYS IXFHFT140N30P). The filter and auxiliary inductors were implemented using the powder cores CH572060 and CM467060, respectively, from Changsung. The auxiliary capacitor C_a and the HVS capacitors C_1 and C_2 were implemented using the film capacitor MHBA035300RSD (ICEL, 500 V, 30 μF). The LVS capacitor C_L was implemented using the film capacitor C4AEGBW6100A3NJ (KEMET, 450 V, 100 μF).

The experimental waveforms for the inductors and switches were measured at full load with $V_L = 116$ V and $V_H = 390$ V. Fig. 10 shows the experimental waveforms of the filter and auxiliary inductor currents, demonstrating forward and backward operations.

Figs. 11 and 12 show the experimental voltage and current waveforms of the switches in the forward and backward modes, respectively. It can be seen that all the switches were turned ON under ZVS in both forward and backward modes.

Fig. 13 shows the experimental waveforms of the battery voltage and current under power flow change, when the LVS of the HSBDC is connected to a lithium iron phosphate battery with nominal voltage of 100 V. It is seen that power flow change of the HSBDC is performed seamlessly in both directions.

In order to demonstrate the advantages of the proposed PPS method over the PWM method presented in [22], experimental comparison between PPS and PWM method is provided.

In the forward mode operation, as we can see in Fig. 14(a) and Table II, both PWM and PPS methods achieve soft-switching under whole load power and voltage gain range, thereby showing

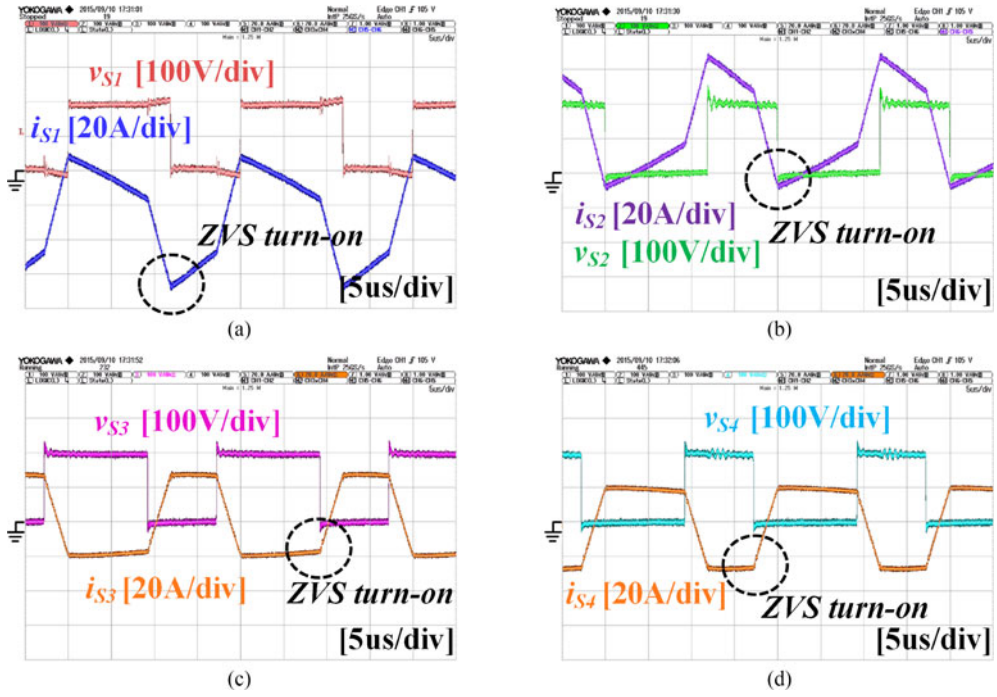

Fig. 12. Experimental waveforms of switch voltage and current in backward mode at full load with $V_L = 116$ V and $V_H = 390$ V. (a) S_1. (b) S_2. (c) S_3. (d) S_4.

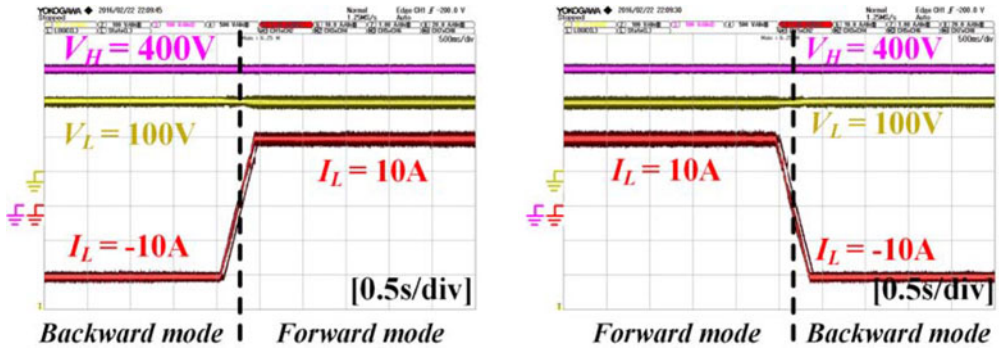

Fig. 13. Experimental waveforms under power flow change. (a) From forward mode to backward mode. (b) From backward mode to forward mode.

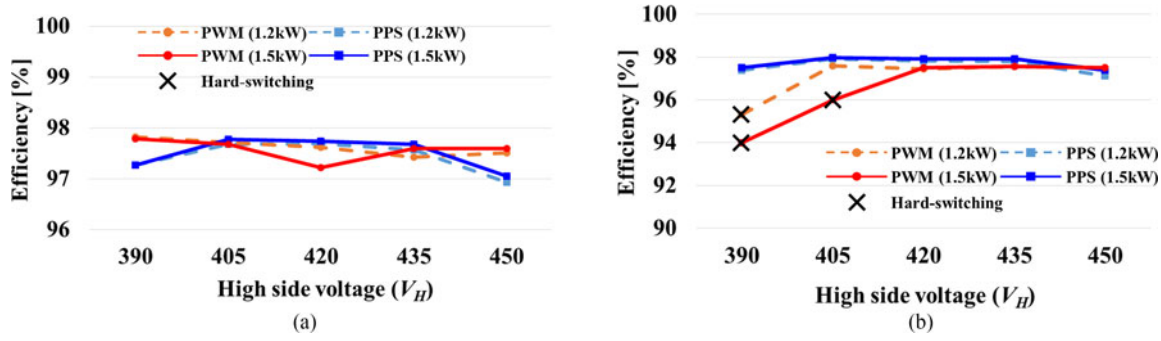

Fig. 14. Measured efficiency of PWM and PPS methods as a function of the high side voltage at $V_L = 86$. (a) Forward mode (b) Backward mode (measured by Yokogawa WT3000).

TABLE II
COMPARISON OF ZVS RANGE OF PWM AND PPS METHODS ACCORDING TO VOLTAGE GAIN AND LOAD POWER

Proposed PPS method	PWM method [22]
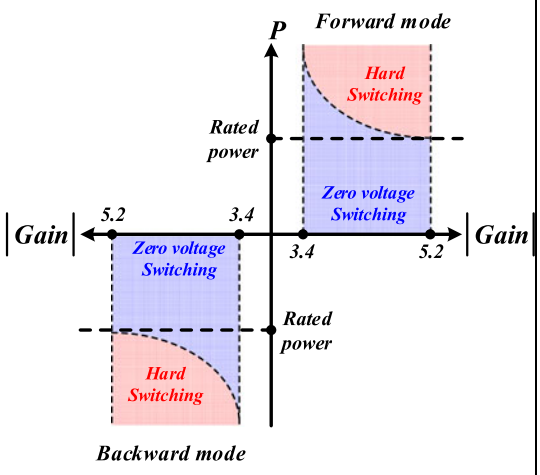 (a)	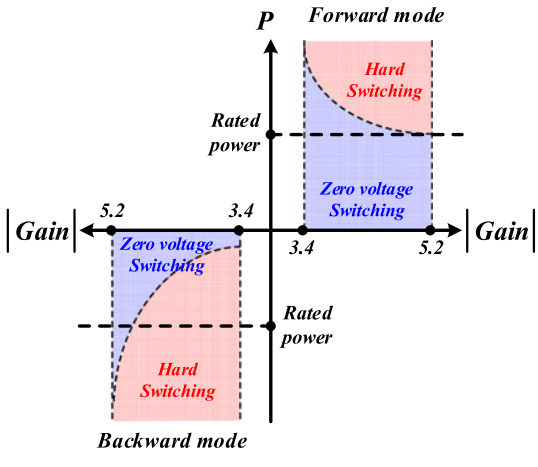 (b)
The proposed PPS method ensures soft-switching both forward and backward modes even under wide voltage range	The PWM method necessitates a sacrifice of soft-switching under wide voltage range.

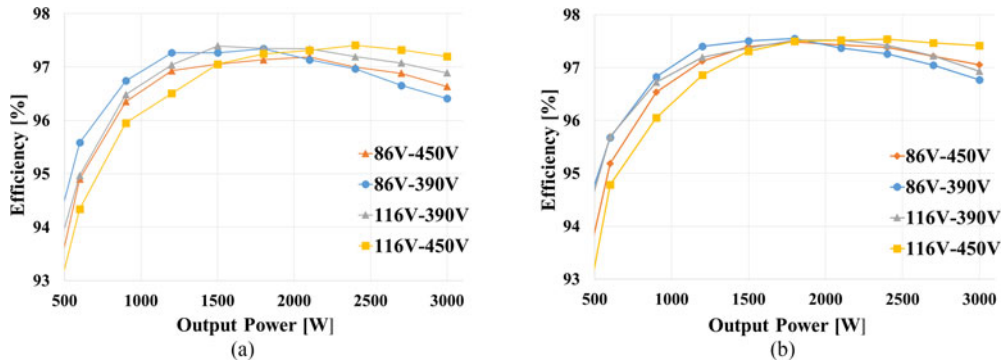

Fig. 15. Measured efficiency of the HSBDC as a function of the output power. (a) Forward mode. (b) Backward mode. (measured by Yokogawa WT3000).

similar measured efficiencies. In the backward mode, as shown in Fig. 14 and Table II, the proposed PPS method also shows high efficiency as it does in the forward mode, achieving soft-switching under whole load power and voltage gain range due to symmetrical operation characteristic. However, in the backward mode, due to unsymmetrical operation characteristic, the ZVS range of the PWM method gets narrower as load power increases or voltage gain decreases, as shown in Fig. 14(b) and Table II, thereby showing much lower efficiency compared to the PPS method.

The measured conversion efficiencies versus the output power for different specifications of voltage in both modes are shown in Fig. 15. It should be noted that the efficiencies are greater than 96% at power levels above 900 W for both forward and backward modes. The maximum efficiencies of the forward and backward mode at 2.4 kW were 97.4% and 97.6%, respectively. A photograph of the prototype of the HSBDC with PPS control is shown in Fig. 16.

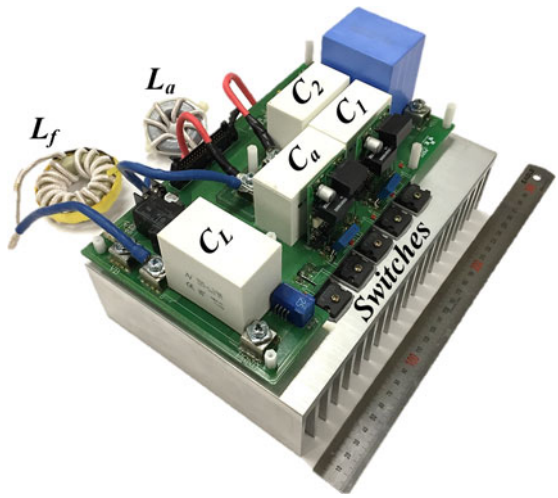

Fig. 16. Photograph of the 3 kW HSBDC prototype.

VI. Conclusion

In this paper, the PPS control for a nonisolated HSBDC was proposed. By utilizing two control parameters, the switching patterns for bidirectional operation of the HSBDC with PPS control become symmetrical, which results in increased design flexibility, seamless power flow change without using complicated control method, increased soft-switching range under wide voltage range, and identical voltage ratings of components. A design guideline of the passive components for ensuring soft-switching at all load power under given voltage range is provided. The experimental results taken from a 3 kW laboratory prototype verified the validity of the HSBDC with PPS control. Power flow change of the HSBDC with PPS control was shown to be seamless in both directions. Note that ZVS turn-on of all switches was achieved at the rated power under whole voltage range. The prototype achieved peak efficiencies of 97.4% and 97.6% in the forward and backward modes, respectively.

References

[1] M. Aamir, S. Mekhilef, and H. J. Kim, "High-gain zero-voltage switching bidirectional converter with a reduced number of switches," *IEEE Trans. Circuits Syst. II, Express Briefs*, vol. 62, no. 8, pp. 816–820, Aug. 2015.

[2] M. Uno and K. Tanaka, "Single switch cell voltage equalizer using multi-stacked buck boost converters operating in discontinuous conduction mode for series connected energy storage cells," *IEEE Trans. Veh. Technol.*, vol. 60, no. 8, pp. 3635–3645, Oct. 2011.

[3] M. Uno and A. Kukita, "Bidirectional PWM converter integrating cell voltage equalizer using series-resonant voltage multiplier for series-connected energy storage cells," *IEEE Trans. Power Electron.*, vol. 30, no. 6, pp. 3077–3090, Jun. 2015.

[4] Y. Hsieh, J. Chen, L. Yang, C. Wu, and W. Liu, "High-conversion-ratio bidirectional DC–DC converter with coupled inductor," *IEEE Trans. Ind. Electron.*, vol. 61, no. 1, pp. 210–222, Jan. 2014.

[5] H. Wu, Y. Xing, Y. Xia, and X. Ma, "A family of non-isolated three-port converters for stand-alone renewable power system," in *Proc. IEEE 37th Annu. Conf. Ind. Electron. Soc.*, 2011, pp. 1030–1035.

[6] F. L. Tofoli, D. de Castro Pereira, W. Josias de Paula, and D. de Sousa Oliveira J´unior, "Survey on non-isolated high-voltage step-up DC–DC topologies based on the boost converter," *IET Power Electron.*, vol. 8, no. 10, pp. 2044–2057, Oct. 2015.

[7] D S. Dwari and L. Parsa, "An efficient high-step-up interleaved DC-DC converter with a common active clamp," *IEEE Trans. Power Electron.*, vol. 26, no. 1, pp. 66–78, Jan. 2011.

[8] C. -C. Lin, L. -S. Yang, and G. Wu, "Study of a non-isolated bidirectional DC–DC converter," *IET Power Electron.*, vol. 6, pp. 30–37, 2013.

[9] F. Z. Peng, F. Zhang, and Z. Qian, "A magnetic-less DC-DC converter for dual-voltage automotive systems," *IEEE Trans. Ind. Appl.*, vol. 39, no. 2, pp. 511–518, Mar./Apr. 2003.

[10] H. S. Chung, A. Ioinovici, and Wai-Leung Cheung, "Generalized structure of bi-directional switched-capacitor dc/dc converters," *IEEE Trans. Circuits Syst. I, Fundam. Theory Appl.*, vol. 50, no. 6, pp. 743–753, Jun. 2003.

[11] H. P. Le, S. R. Sanders, and E. Alon, "Design techniques for fully integrated switched-capacitor DC–DC converters," *IEEE Trans. Solid-State Circuits*, vol. 46, no. 9, pp. 2120–2131, Sep. 2011.

[12] W. Qian, D. Cao, J. G. Cintron-Rivera, M. Gebben, D. Wey, and Z. P. Fang, "A switched-capacitor DC–DC converter with high voltage gain and reduced component rating and count," *IEEE Trans. Ind. Appl.*, vol. 48, no. 4, pp. 1397–1406, Jul./Aug. 2012.

[13] B. L. Narasimharaju, S. P. Dubey, and S. P. Singh, "Coupled inductor bidirectional DC-DC converter for improved performance," in *Proc. IEEE Int. Conf. Ind. Electron., Control Robot.*, 2010, pp. 28–33.

[14] B. L. Narasimharaju, S. P. Dubey, and S. P. Singh, "Design and analysis of coupled inductor bidirectional DC-DC convertor for high-voltage diversity applications," *IET Power Electron.*, vol. 5, no. 7, pp. 998–1007, Aug. 2012.

[15] M. N. Gitau, F. M. Mwaniki, and I. W. Hofsajer, "Analysis and design of a single-phase tapped-coupled-inductor boost DC–DC converter," *J. Power Electron.*, vol. 13, no. 4, pp. 636–646, Jul. 2013.

[16] E. Dimopoulos and S. Munk-Nielsen, "A tapped-inductor buck-boost converter for a dielectric electroactive polymer generator," in *Proc. 29th IEEE Appl. Power Electron. Conf. Expo.*, 2014, pp. 3125–3131.

[17] J. Yao, A. Abramovitz, and K. M. Smedley, "Steep-gain bidirectional converter with a regenerative snubber," *IEEE Trans. Power Electron.*, vol. 30, no. 12, pp. 6845–6856, Dec. 2015.

[18] T. J. Liang, H. H. Liang, S. M. Chen, J. F. Chen, and L. S. Yang, "Analysis, design, and implementation of a bidirectional double-boost DC-DC converter," *IEEE Trans. Ind. Appl.*, vol. 50, no. 6, pp. 3955–3962, Nov./Dec. 2014.

[19] J. Chen, D. Sha, Y. Yan, B. Liu, and X. Liao, "Cascaded high voltage conversion ratio bidirectional non-isolated DC-DC converter with variable switching frequency," *IEEE Trans. Power Electron.*, to be published.

[20] I. O. Lee, S. Y. Cho, and G.W. Moon, "Interleaved buck converter having low switching losses and improved step-down conversion ratio," *IEEE Trans. Power Electron.*, vol. 27, no. 8, pp. 3664–3675, Aug. 2012.

[21] H. Wu, K. Sun, L. Chen, L. Zhu, and Y. Xing, "High step-up/step-down soft-switching bidirectional DC–DC converter with coupled-inductor and voltage matching control for energy storage systems," *IEEE Trans. Ind. Appl.*, vol. 63, no. 5, pp. 2892–2903, May 2016.

[22] M. Kwon and S. Choi, "High gain soft-switching bidirectional DC–DC converter for eco-friendly vehicles," *IEEE Trans. Power Electron.*, vol. 29, no. 4, pp. 1659–1666, Apr. 2014.

Hyeonju Jeong was born in South Korea, in 1989. He received the B.S. degree from the Department of Electronics and Electrical Engineering, Dankook University, Yongin, South Korea, in 2014, and the M.S. degree from the Department of Electrical and Information Engineering, Seoul National University of Science and Technology (Seoul Tech), Seoul, South Korea, in 2016. He is currently working toward the Ph.D. degree in electrical and information engineering at Seoul Tech.

His research interests include bidirectional dc–dc converter and resonant converter for electric vehicles and renewable energy systems.

Minho Kwon was born in South Korea, in 1985. He received the B.S. and M.S. degrees in control and instrumentation engineering, in 2012 and 2014, respectively, from Seoul National University of Science and Technology (Seoul Tech), Seoul, South Korea, where he is currently working toward the Ph.D. degree in electrical and information engineering.

His research interests include bidirectional dc–dc converter and grid-connected inverter for electric vehicles and renewable energy systems.

Sewan Choi (S'92–M'96–SM'04) received the B.S. degree in electronic engineering from Inha University, Incheon, South Korea, in 1985, and the M.S. and Ph.D. degrees in electrical engineering from Texas A&M University, College Station, TX, USA, in 1992 and 1995, respectively.

From 1985 to 1990, he was with Daewoo Heavy Industries as a Research Engineer. From 1996 to 1997, he was a Principal Research Engineer with Samsung Electro-Mechanics Co., South Korea. In 1997, he joined the Department of Electrical and Information Engineering, Seoul National University of Science and Technology (Seoul Tech), Seoul, South Korea, where he is currently a Professor. His research interests include power conversion technologies for renewable energy systems and dc–dc converters and battery chargers for electric vehicles.

Dr. Choi is an Associate Editor of the IEEE Transactions on Power Electronics and the IEEE Journal on Emerging and Selected Topics in Power Electronics.